sciendo Journal of Electrical Engineering, Vol. 76, No. 4, 2025, pp. 370-376

Enhanced inductive post design for H-plane T-junction power dividers in reduced-height waveguide

Nguyen Tuan Hung[1], Nguyen Minh Giang[1], Pham Hoang Long[2], Nguyen Thanh[2]

This paper presents an enhanced inductive post structure for H-plane T-junction power dividers implemented in reduced-height rectangular waveguides. By incorporating one or two additional circular disks into the conventional cylindrical post, the proposed design introduces extra degrees of freedom for impedance tuning, thereby enabling improved matching performance for both single-frequency and broadband designs. Simulation and measurement results confirm that the proposed structure achieves excellent impedance matching and broadband performance within the Ku-band, demonstrating strong potential for integration into high-performance RF systems requiring compact size, low loss, and wide bandwidth.

Keywords: broadband, power divider, T-junction, inductive post, waveguide, optimization

1 Introduction

RF power dividers are indispensable components in communication, radar, and instrumentation systems and subsystems [1-18]. Three common technologies for designing RF power dividers are based on waveguides (WG) [1, 3, 4, 6-10], microstrip lines (MSL) [11-13], and substrate integrated waveguides (SIW) [14-16]. Compared to MSL and SIW dividers, the primary disadvantage of WG power dividers is their relatively large physical size, but they can offer the significant advantages of low insertion loss and high-power handling capability. High-performance WG power dividers are typically realized using techniques such as incorporating an inductive post [3, 4], or a wedge with an inductive window [1, 6-10] within an H-plane T-junction. The characteristics of inductive posts have been extensively analyzed in [2, 4, 5], and particularly in [4], their effectiveness in T-junctions has been demonstrated by calculating a scale model in the C-band to predict performance in the X-band using standard WG dimensions (WR229). On the other hand, although WGs are generally designed in standard sizes [1, 3, 4], certain applications, such as transitions or feeding networks for WG antennas [6-10, 17, 18], may benefit from non-standard configurations, such as reduced-height WGs. Although the reduced-height designs of WG may lead to increased insertion loss (as illustrated in Fig. 1), they can help minimize the overall system size effectively. Besides, for WG T-junctions, existing studies have not yet explored the use of any inductive posts in reduced-height configurations.

In this study, we propose an enhanced inductive post structure for use in an H-plane T-junction power divider based on a reduced-height WG. Specifically, the design involves adding one or two circular disks to the post, thereby increasing properly the number of design parameters and allowing greater flexibility in optimizing the T-junction's performance. As will be demonstrated, the proposed structure enables excellent impedance matching either at a specific frequency or over a wide bandwidth covering the Ku-band (12.4-18 GHz), depending on the design case.

2 Conventional and proposed post structures for T-junction designs in reduced-height WGs

2.1 Insertion loss of reduced-height WGs

As illustrated in Fig. 1, reducing the height of the waveguide (WG) from its standard dimension increases the insertion loss. In CST simulations, a WR62 transmission line (15.8×7.9 mm) with a length of 77.5 mm was used. When the height was reduced from 7.9 mm to 1 mm while maintaining the width at 15.8 mm, the insertion loss increased in Ku-band, for example, from 0.02 dB to 0.1 dB at 15 GHz. This indicates that designs utilizing reduced-height WR62 waveguides inherently face the challenge of increased loss. It should be noted, however, that the cut-off frequency f_c of the dominant TE_{10} mode remains unchanged, as it is given by:

$$f_c = \frac{c}{2a} = \frac{3\times10^8}{2\times15.8\times10^{-3}} \approx 9.49\,(\text{GHz}) \tag{1}$$

Accordingly, the guided wavelength at a specific frequency f_0, determined by:

[1] Faculty of Radio-Electronic Engineering, Le Quy Don Technical University, Ha Noi 100000, Vietnam
[2] Research Institute of Posts and Telecommunications, Posts and Telecommunications Institute of Technology, Ha Noi 100000, Vietnam
Corresponding author's email: thanhn@ptit.edu.vn

https://doi.org/10.2478/jee-2025-0038, Print (till 2015) ISSN 1335-3632, On-line ISSN 1339-309X

$$\lambda_g = \frac{\lambda_0}{\sqrt{1-\left(\frac{\lambda_0}{\lambda_c}\right)^2}} = \frac{\lambda_0}{\sqrt{1-\left(\frac{f_c}{f_0}\right)^2}} \tag{2}$$

is not affected by reduced-height of WR62. Therefore, the primary issue associated with using reduced-height WGs is the increase in insertion loss. Minimizing this loss becomes a critical design consideration, particularly in systems that demand extremely low-loss performance.

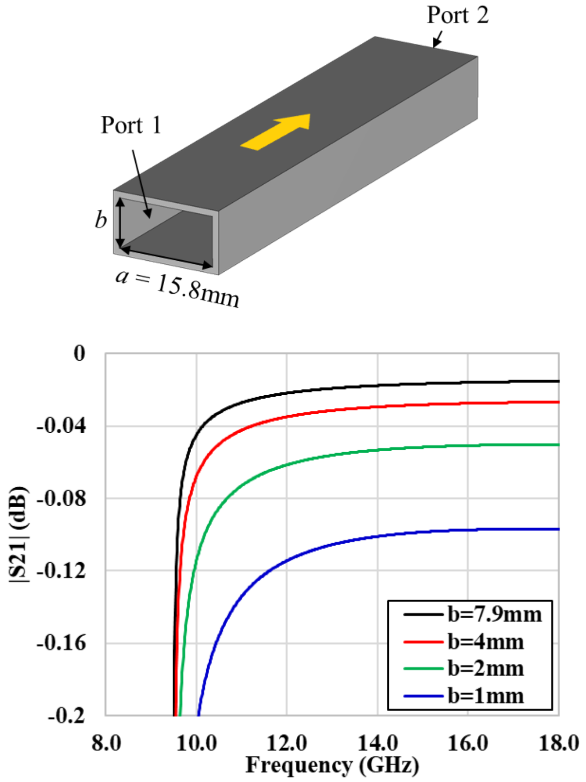

Fig. 1. Insertion loss of reduced-height versions of WR62

2.2 Conventional post structure

Figure 2 shows a T-junction constructed on a reduced-height version of WR62, specifically, an approximately half-height WG (15.8×4.0 mm), and its scattering matrix's magnitudes before and after loading a cylindrical post in the conventional design. The analysis of such a post was first detailed in [2], and later successfully applied for WG T-junctions in [4]. A similar technique can also be extended to substrate integrated waveguide (SIW) T-junctions, as demonstrated in [15, 16]. Here, the initial values of the post diameter $d_p = 2$ mm and its offset to the WG wall $l = 6.45$ mm are chosen based on the recommendations in [4]. As shown in Fig. 2, the effectiveness of the inductive post is clearly demonstrated across a wide frequency range. Specifically, it improves both the return loss and insertion loss, such that |S11| remains below –9.8 dB and |S21| exceeds –3.5 dB throughout the entire Ku-band. In contrast, without the post, the corresponding values are significantly worse, with a minimum |S11| of only –5.2 dB and a maximum |S21| of –4.6 dB.

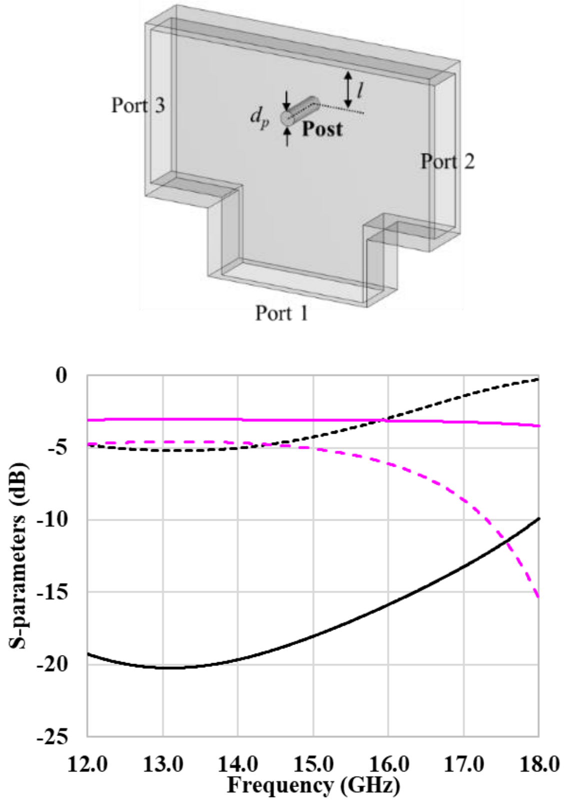

Fig. 2. Half-height WG T-junction with (Model 1) or without an inductive post

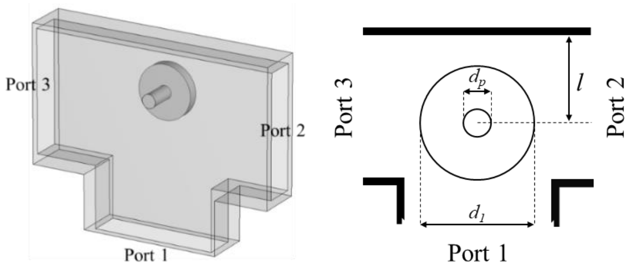

(a) Model 2

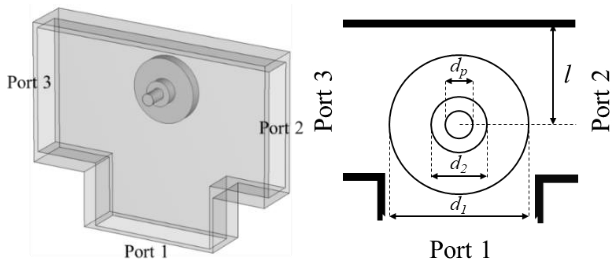

(b) Model 3

Fig. 3. Proposed design with enhanced inductive post structures

2.3 Proposed post structure

As shown in Fig. 2, the conventional design of the post (Model 1) has only two design parameters (d_p, l). Consequently, optimizing the T-junction performance using this configuration is limited by the small number of adjustable parameters, as will be demonstrated in the subsequent results. To address this limitation, we propose novel post structures that introduce additional degrees of freedom, thereby enabling improved performance optimization. Specifically, the technique is to add one or two circular disks as depicted by Model 2 and Model 3 in Fig. 3 where they have three (d_p, d_1, l), or four (d_p, d_1, d_2, l) design parameters, respectively.

In the following subsections, we focus on the performance optimization of all three models Model 1 (Fig. 2), Model 2, and Model 3, and compare their design effectiveness in two scenarios: optimization over the full Ku-band, and optimization targeting a specific frequency within the Ku-band.

2.3.1 Optimization in the entire Ku-band

Since all T-junction models considered in this study function as equal power dividers with negligible conductor loss, the optimization primarily focuses on improving the return loss in CST simulations. For broadband impedance matching over the entire Ku-band, the worst-case return loss, defined as the maximum value of |S11| (in dB) within the Ku-band, is used as the performance criterion. Accordingly, the objective function for broadband optimization, denoted as OF_a, is defined as:

$$OF_a = \max_{f\in[12.4,18]\,\mathrm{GHz}} \left(|S11(f)| \right) \tag{3}$$

Table 1. Optimized design parameters of three models in the entire Ku-band (Unit: mm)

	d_p	l	d_1	d_2
Model 1	1.420	6.491		
Model 2	1.515	6.744	7.235	
Model 3	1.556	6.823	8.922	2.782

In each model, by minimizing OF_a as small as possible, we will obtain the optimum values of (d_p, l) for Model 1, or (d_p, d_1, l) for Model 2, or (d_p, d_1, d_2, l) for Model 3. The resulting S-parameter comparisons after optimization are presented in Fig. 4, while the corresponding optimized parameter values are listed in Table 1. In Fig. 4(a), the worst values of |S11| in the entire Ku-band of each model are:

$$OF_{a\text{-}Model1} = \max(|S11|)_{Model1} = -14.1\text{ dB} >$$
$$OF_{a\text{-}Model2} = \max(|S11|)_{Model2} = -17.8\text{ dB} >$$
$$OF_{a\text{-}Model3} = \max(|S11|)_{Model3} = -19.0\text{ dB}$$

Meanwhile, in Fig. 4(b), their worst values of |S21| in the entire Ku-band are:

$\min(|S21|)_{Model1} = -3.20$ dB $< \min(|S21|)_{Model2} = -3.11$ dB $< \min(|S21|)_{Model3} = -3.08$ dB

These results clearly demonstrate that both Model 2 and Model 3 outperform Model 1 in terms of broadband impedance matching and low-loss performance, with Model 3 achieving the best overall performance across the entire Ku-band.

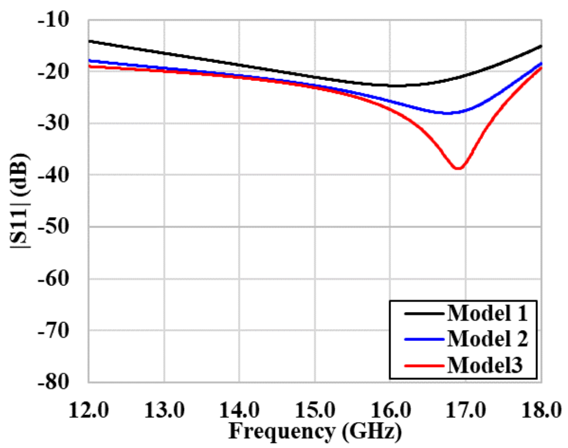

(a) Return loss

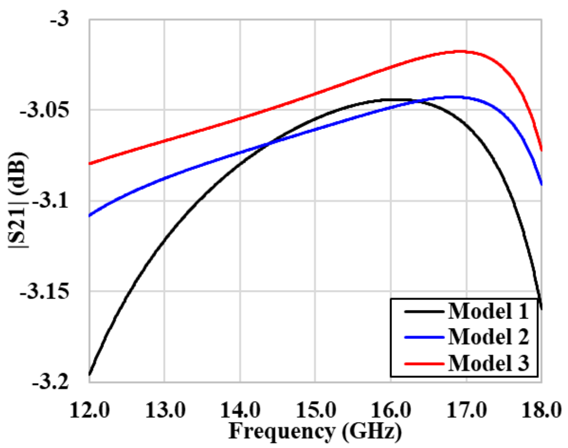

(b) Insertion loss

Fig. 4. Comparison of S-parameters between three models when optimizing the bandwidth

2.3.2 Optimization at a specific frequency within Ku-band

For the optimization at a specific frequency within Ku-band, for example, at $f_0 = 15$ GHz, the objective function OF_b is simply defined as the return loss at that frequency:

$$OF_b = |S11(f_0)| = |S11|@15\text{GHz} \qquad (4)$$

Table 2. Optimized design parameters of three models at 15 GHz (unit: mm)

	d_p	l	d_1	d_2
Model 1	1.420	6.491		
Model 2	1.515	6.744	7.235	
Model 3	1.556	6.823	8.922	2.782

Similar to the previous optimization cases of OF_a in Eqn. (3), minimizing OF_b yields the optimum values of (d_p, l) for Model 1, or (d_p, d_1, l) for Model 2, or (d_p, d_1, d_2, l) for Model 3, which enable each model to achieve the best response at the center frequency of 15 GHz. Figure 5 shows the comparison of S-parameters between the three models after optimization, and their optimized design parameters are listed in Table 2. In Fig. 5(a), the best values of |S11| at 15 GHz of each model are:

$$OF_{b\text{-Model1}} = \min(|S11|)_{\text{Model1}} = -24.8 \text{ dB} >$$
$$OF_{b\text{-Model2}} = \min(|S11|)_{\text{Model2}} = -45.6 \text{ dB} >$$
$$OF_{b\text{-Model3}} = \min(|S11|)_{\text{Model3}} = -69.3 \text{ dB}$$

Accordingly, in Fig. 5(b), their best values of |S21| at 15 GHz are maximized to $\max(|S21|)_{\text{Model1}} = -3.04$ dB < $\max(|S21|)_{\text{Model2}} = -3.03$ dB < $\max(|S21|)_{\text{Model3}} = -3.02$ dB. These results clearly indicate that Models 2 and 3 are better than Model 1 in terms of impedance matching and transmission at 15 GHz, with Model 3 again exhibiting the best performance.

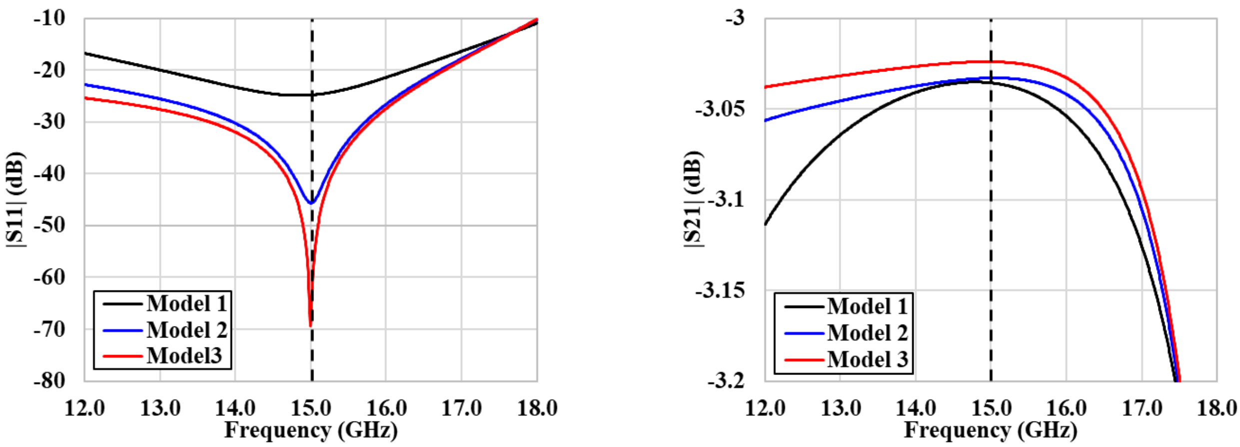

(a) Return loss (b) Insertion loss

Fig. 5. Comparison of S-parameters between three models when optimizing the impedance matching at 15 GHz

Figure 6 illustrates the electric field distribution of the three models, where red indicates strong field intensity, yellow and green denote moderate levels, and blue represents weak field regions. By observing the area between the input port (Port 1) and the post in each model, it is evident that Model 1 exhibits the strongest reflected electric field, indicating a high reflection coefficient (|S11|), which is undesirable. In Model 2, the electric field is partially concentrated around the circular disc, suggesting that some energy is effectively coupled into the structure. This implies improved impedance matching and lower reflection compared to Model 1. In Model 3, the reflected field in the observed region is significantly minimized. The presence of the improved post further enhances impedance matching, as evidenced by the more concentrated and well-directed electric field around the discs, with minimal back-reflection. These qualitative observations indicate that Model 3 achieves the best reflection performance (i.e., lowest |S11| at 15 GHz) among the three, followed by Model 2, which also outperforms the conventional configuration of Model 1.

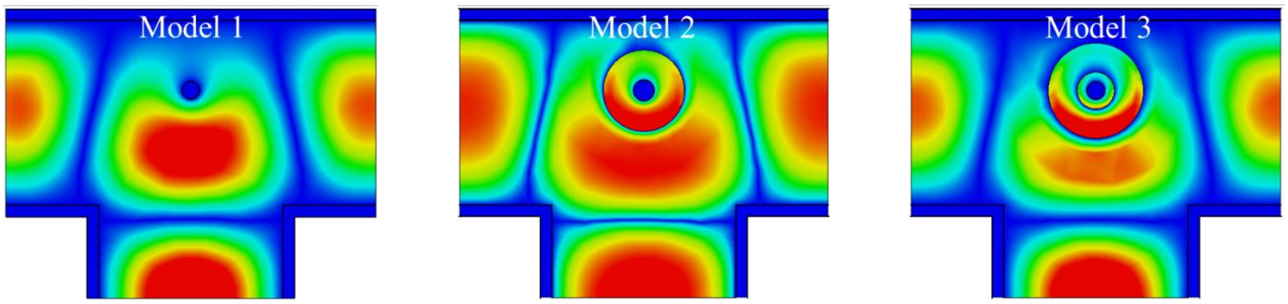

(a) Model 1 (b) Model 2 (c) Model 3

Fig. 6. Comparison of electric field distribution of three models at 15 GHz

Table 3. Comparison of the T-junctions in [4] and Model 3 in this work

Ref.	WG type	Bandwidth of |S11| ≤ –20 dB	Bandwidth of |S11| ≤ –30 dB	Minimum |S11| (dB)	Maximum |S21| (dB)
[4]	Standard WR229	> 17.7%	4.1% (3.80-3.96 GHz)	–36 (3.90 GHz)	N/A
This work (2.3.1)	Half-height WR62	31.6% (13.05-17.95 GHz)	6.2% (16.30-17.34 GHz)	–38.8 (16.69 GHz)	–3.02 (16.69 GHz)
This work (2.3.2)	Half-height WR62	29.9% (12.40-16.77 GHz)	14.6% (13.65-15.80 GHz)	–69.3 (15.00 GHz)	–3.02 (15.00 GHz)

On the other hand, as observed again in Fig. 5(a), although the optimization in subsection 2.3b targets impedance matching only at 15 GHz, Model 3 still retains a broadband response. Detailed comparative data between the performance of Model 3 and that of previously reported T-junctions in [4] are summarized in Tab. 3, clearly demonstrating the wideband and low-loss characteristics of the proposed structure. It is also noteworthy from Table 3 that, within the Ku-band, the version of Model 3 optimized over the full Ku-band (subsection 2.3a) achieves a wider bandwidth of |S11| ≤ –20 dB than the version optimized at a single frequency (subsection 2.3.2).

3 Fabrication and measurement

To validate the simulation results, the proposed Model 3 of the T-junction in subsection 2.3.2 was fabri-cated using aluminum alloy, as shown in Fig. 7. Unlike the simulated version, the output arms of the T-junction were bent and secured with additional screws to improve structural robustness and mechanical stabi-lity during handling and measurement. For experimental validation with a Vector Network Analyzer (VNA), three coaxial-to-waveguide (SMA to half-height WR62) transitions were used to connect standard SMA cables to the half-height WR62 waveguide ports. These transi-tions are labeled as Transition 1, Transition 2, and Transition 3, corresponding to the three waveguide ports, as shown in Fig. 8. The measurement setup in Fig. 8 illustrates a typical test configuration in which Port 1 is used as the input, Port 2 as the output, and Port 3 is terminated with a 50 Ω load.

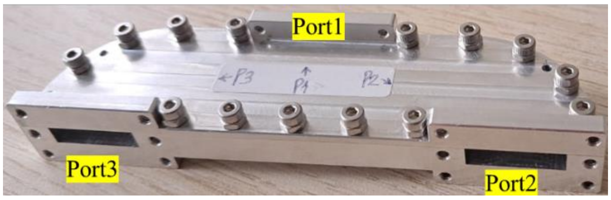

(a) Top view

(b) Front view

Fig. 7. Fabricated T-junction (Model 3) for measurement

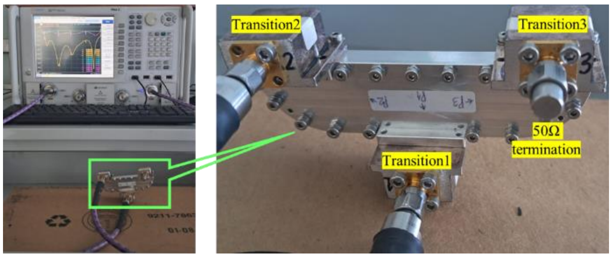

Fig. 8. Measurement setup for the fabricated T-junction with three coaxial-waveguide transitions

Figure 9 presents the measured S-parameters of the fabricated T-junction (Model 3) and compares them with simulated results. As shown in Fig. 9(a), the simulated reflection coefficient |S11| exhibits a deep null of approximately –70 dB at 15 GHz, indicating excellent impedance matching, and the measured |S11| also demonstrates a pronounced dip below –45 dB at the same frequency, confirming the strong agreement between simulation and measurement at the center frequency. Although small discrepancies of |S11| are observed at lower and higher frequencies, the measured result still demonstrates a broad low-reflection bandwidth within the Ku-band. Specifically, the bandwidths for |S11| ≤ –10 dB (VSWR ≤ 2) and |S11| ≤ –14 dB (VSWR ≤ 1.5) are 35.4% (12.38-17.70 GHz) and 28.2% (13.14-17.46 GHz), respectively. On the other hand, both the simulated and measured results of transmission coefficient magnitude |S21| remains relatively flat around –3.0 dB across the Ku-band, indicating low insertion loss and efficient power transfer. The largest deviation of |S21| between simulated and measured results within Ku-band occurs at the lower frequency end of 12.4 GHz, but it is very small. Overall, the observed differences in both |S11| and |S21| are primarily attributed to fabrication tolerances, surface roughness, and, most notably, the influence of the transitions.

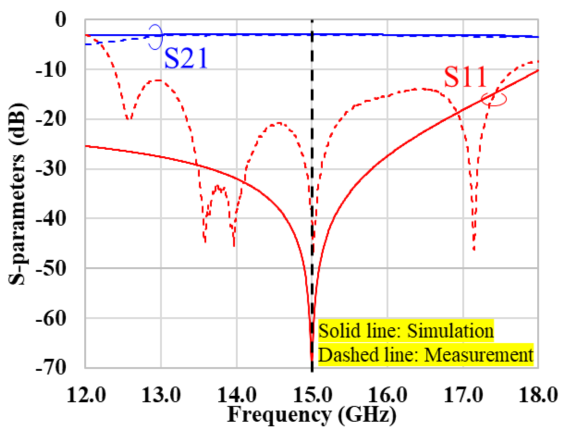

(a) Simulation vs. measurement

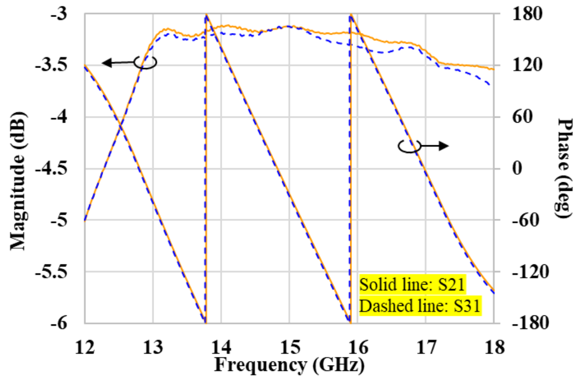

(b) Measured S21 vs. S31

Fig. 9. Measurement results of S-parameters

Figure 9(b) further illustrates the measured magnitudes and phases of S21 and S31, corresponding to the two output ports. The magnitude curves are nearly symmetrical, with values between –4.3 dB and –3.1 dB in the Ku-band, and reach –3.1 dB at 15 GHz, suggesting excellent balanced power division. Additionally, the measured phase difference between S21 and S31 remains extremely small and stable over the full frequency band, confirming the symmetry of the divider and minimal phase imbalance. These results validate the proposed design's effectiveness, demonstrating good matching, low-loss, and equal power split across the Ku-band, particularly around the center frequency of 15 GHz.

4 Conclusion

This paper has introduced an enhanced inductive post design for H-plane T-junction power dividers based on half-height WR62 operating in Ku-band. By adding circular disks into the cylindrical post, the proposed method enables greater control over impedance characteristics, supporting both full band and single-frequency optimizations. The design achieves a compact form factor while maintaining low reflection and balanced output performance. Results in simulation and experimental validation confirm the feasibility and effectiveness of the proposed design, demonstrating improved impedance matching and broadband characteristics compared to conventional method. The proposed technique is particularly promising for integration into high-frequency systems where broadband and low-loss characteristics are critical, such as compact WG transitions and antenna feeding networks. This technique however cannot be directly applied to SIW power dividers. Therefore, further investigation into alternative configurations that are compatible with SIW technology would be a valuable direction for future research.

Acknowledgement

This work was supported by Le Quy Don Technical University under project number 25.01.41.

References

[1] T. Li, W. Dou, and H. Meng, "Broadband power divider based on waveguide T-junctions at Ka-band," *IEICE Electronics Express*, vol. 13, no. 4, pp. 1–7, Jan. 2016. doi:10.1587/elex.13.20150992.

[2] Y. Leviatan, P. G. Li, A. T. Adams, and J. Perini, "Single-post inductive obstacle in rectangular waveguide," *IEEE Trans. Microwave Theory Tech.*, vol. 31, no. 10, pp. 806–812, Oct. 1983. doi:10.1109/TMTT.1983.1131610.

[3] A. R. Akbarzadeh and Z. X. Shen, "Waveguide power dividers using multiple posts," *Microwave and Optical Technology Letters*, vol. 50, no. 4, pp. 981–984, Apr. 2008. doi:10.1002/mop.23259.

[4] J. Hirokawa, K. Sakurai, M. Ando, and N. Goto, "An analysis of a waveguide T-junction with an inductive post," *IEEE Trans. Microwave Theory Tech.*, vol. 39, no. 3, pp. 563–567, Mar. 1991. doi: 10.1109/22.75301.

[5] K. Li Wu and H. Y. Wang, "A rigorous modal analysis of H-plane waveguide T-junction loaded with a partial-height post for wide-band applications," *IEEE Trans. Microwave Theory Tech.*, vol. 49, no. 5, pp. 893–901, May 2001. doi:10.1109/22.920146.

[6] G. L. Huang, S. G. Zhou, T. H. Chio, and T. S. Yeo, "Design of a symmetric rectangular waveguide T-junction with in-phase and unequal power split characteristics," *2013 IEEE Antennas and Propagation Society International Symposium (APSURSI)*, Orlando, FL, USA, Jul. 2013, pp. 2119–2120. doi:10.1109/APS.2013.6711718.

[7] G. L. Huang, S. G. Zhou, and T. H. Chio, "Development of a symmetric waveguide T-junction power divider with equal-phase characteristic," *ACES Journal*, vol. 31, no. 3, pp. 309–314, Mar. 2016.

[8] G. L. Huang, S. G. Zhou, T. H. Chio, H. T. Hui, and T. S. Yeo, "A low profile and low sidelobe wideband slot antenna array fed by an amplitude-tapering waveguide feed-network," *IEEE Trans. Antennas Propag.*, vol. 63, no. 1, pp. 419–423, Oct. 2014. doi:10.1109/TAP.2014.2365238.

[9] H. Yuan, J. Li, Z. Zhao, Z. Wang, M. B. Lodi, G. Gugliandolo, N. Donato, G. Crupi, L. Si, and X. Bao, "Development of a wideband slotted antenna array with low profile and low sidelobe," *Electronics*, vol. 12, no. 2, Art. 278, Jan. 2023. doi:10.3390/electronics12020278.

[10] P. Liu, G. F. Pedersen, and S. Zhang, "Wideband low sidelobe slot array antenna with compact tapering feeding network for E-band wireless communications," *IEEE Trans. Antennas Propag.*, vol. 70, no. 4, Apr. 2022. doi: 10.1109/TAP.2021.3119030.

[11] M. G. Nguyen, C. T. N. Nguyen, T. H. Nguyen, and H. Morishita, "Design of a dual-band three-way power divider with unequally high power split ratio," *Radio Engineering*, vol. 32, no. 3, pp. 338–344, Sep. 2023. doi:10.13164/re.2023.0338.

[12] M. G. Nguyen, H. M. T. Le, D. M. Le, and T. T. H. Tran, "A simple design of low-loss quad-band Wilkinson power dividers," *Journal of Electrical Engineering*, vol. 75, no. 1, pp. 63–71, Jan. 2024. doi:10.2478/jee-2024-0009.

[13] O. Kasar, "A low profile compact three-way Wilkinson power divider with size reduction," *Journal of Electrical Engineering*, vol. 71, no. 6, pp. 419–422, Dec. 2020. doi: https://doi.org/10.2478/jee-2020-0057.

[14] V. T. Mai, T. H. Nguyen, K. P. Kieu, T. T. H. Tran, T. L. Nguyen, C. H. Ta, and D. M. Luong, "An improved filtering power divider using substrate integrated waveguide for Ku-band satellite applications," *Int. J. RF Microwave Comput.-Aided Engr.*, vol. 2025, no. 1, pp. 1–8, Feb. 2025. doi:10.1155/mmce/5905191.

[15] S. H. Shehab, N. C. Karmakar, and J. Walker, "Substrate-integrated-waveguide power dividers: An overview of the current technology," *IEEE Antennas Propag. Mag.*, vol. 62, no. 4, pp. 27–38, Aug. 2020. doi:10.1109/MAP.2019.2943308.

[16] F. Bilawal, F. Babaeian, K. T. Trinh, and N. C. Karmakar, "The art of substrate-integrated-waveguide power dividers," *IEEE Access*, vol. 11, pp. 9311–9325, Jan. 2023. doi:10.1109/ACCESS.2023.3239917.

[17] B. Dansran, S. Y. Xu, J. W. Heo, C. S. Lee, and B. C. Ahn, "Design of a broadband transition from a coaxial cable to a reduced-height rectangular waveguide," *Applied Sciences*, vol. 13, no. 20, Art. 11265, Oct. 2023. doi:10.3390/app132011265.

[18] H. S. Oh and K. W. Yeom, "A full Ku-band reduced-height waveguide-to-microstrip transition with a short transition length," *IEEE Trans. Microwave Theory Tech.*, vol. 58, no. 9, pp. 2456–2462, Sep. 2010. doi: 10.1109/TMTT.2010.2058251.

Nguyen Tuan Hung is currently a senior lecturer with the Le Quy Don Technical University, Vietnam.

Nguyen Minh Giang is currently a senior lecturer with the Le Quy Don Technical University, Vietnam.

Pham Hoang Long is currently a researcher with the Posts and Telecommunications Institute of Technology, Vietnam.

Nguyen Thanh is the corresponding author, and currently a researcher with the Posts and Telecommunications Institute of Technology, Vietnam.

Received 13 May 2025